How is the ocean filled?

Geoffrey Gebbie[1] and Peter Huybers[2]

Received 13 January 2011; revised 4 February 2011; accepted 15 February 2011; published 23 March 2011.

[1] The ocean surface rapidly exchanges heat, freshwater, and gases with the atmosphere, but once water sinks into the ocean interior, the inherited properties of seawater are closely conserved. Previous water-mass decompositions have described the oceanic interior as being filled by just a few different property combinations, or water masses. Here we apply a new inversion technique to climatological tracer distributions to find the pathways by which the ocean is filled from over 10,000 surface regions, based on the discretization of the ocean surface at 2° by 2° resolution. The volume of water originating from each surface location is quantified in a global framework, and can be summarized by the estimate that 15% of the surface area fills 85% of the ocean interior volume. Ranked from largest to smallest, the volume contributions scaled by surface area follow a power-law distribution with an exponent of -1.09 ± 0.03 that appears indicative of the advective-diffusive filling characteristics of the ocean circulation, as demonstrated using a simple model. This work quantifies the connection between the surface and interior ocean, allowing insight into ocean composition, atmosphere-ocean interaction, and the transient response of the ocean to a changing climate.
Citation: Gebbie, G., and P. Huybers (2011), How is the ocean filled?, *Geophys. Res. Lett.*, *38*, L06604, doi:10.1029/2011GL046769.

1. Introduction

[2] Traditionally, a handful of water masses having distinct hydrographic properties are called upon to describe the composition of the ocean [e.g., *Wüst*, 1935; *Warren*, 1981], where each water mass is defined by a characteristic set of temperature, salinity, and other hydrographic properties. The oceanic volume occupied by each water mass is typically estimated by inverting hydrographic measurements [e.g., *Tomczak*, 1981; *Mackas et al.*, 1987; *Tomczak and Large*, 1989], but the results have proven sensitive to the number and definition of the water masses. For example, *Broecker et al.* [1998] used one hydrographic property to distinguish between North Atlantic Deep Water and Antarctic Bottom Water, finding that they contributed equally to filling the deep Pacific. More recently, *Johnson* [2008] decomposed the subthermocline world ocean into seven water masses and found that Antarctic Bottom Water fills two to three times more of the deep Pacific than North Atlantic Deep Water. Another answer might be obtained if more water masses were included, but traditional inverse approaches are limited to distinguishing only as many water masses as there are distinct water properties, and there is little prospect of obtaining enough well-measured global tracers to resolve this issue using previous methods.

2. Method

[3] To circumvent this methodological roadblock, we extend and apply a recently developed inverse technique [*Gebbie and Huybers*, 2010], referred to as Total Matrix Intercomparison (TMI). Like other water mass decompositions [e.g., *Tomczak*, 1999], TMI is based upon inverting tracer conservation equations, but it is unique to this class of methods in that it also accounts for the geography interconnecting the tracer observations in a more complete way. More specifically, TMI diagnoses the pathways that connect each interior box to every surface region of a discretized ocean by following trails of similar water properties, where directionality is determined using the telltale signs of nutrient remineralization. Instead of solving for water masses that are defined by water properties, we seek a solution in terms of water origins, where we distinguish waters last in contact with a specific surface region of the ocean. TMI yields an estimate of the interior ocean volume filled from every surface gridbox resolved in a given dataset, thus permitting a more detailed quantification than previously available from observations.

[4] Each surface box is a source of water with a particular set of property values, and as such, can be considered a "water type" as defined by *Tomczak and Large* [1989]. Many surface boxes have similar properties, and thus, interior ocean waters cannot be distinguished by these relatively minor differences. The crucial additional step in this study is to identify waters by their surface origin, and to trace the constituents of each interior water back to the surface location from which they originated. The degree to which waters from adjacent locations can be distinguished is addressed later.

[5] The information content in TMI is encapsulated in the pathways matrix, **A**, derived fully by *Gebbie and Huybers* [2010] and reviewed here. To obtain the matrix, we first solve for the mass contribution made to each box by each of its immediate neighbors using the same form as a traditional water-mass decomposition. In steady state, the tracer concentration in each box must satisfy, $c_o = m_1 c_1 + m_2 c_2 + \ldots + q$, where the m's give the fractional mass contribution and q represents internal sources for nonconservative tracers, related by stoichiometric ratios of 1:15.5:-170 for phosphate, nitrate, and oxygen concentrations [*Anderson and Sarmiento*, 1994]. Each box has up to six neighbors and a biological source term, giving seven unknowns constrained by the six observed tracers and mass conservation. For ease of notation, the m_i and q unknown terms are combined in the vector, **x**. Using a weighted, tapered, non-negative least squares

[1]Department of Physical Oceanography, Woods Hole Oceanographic Institution, Woods Hole, Massachusetts, USA.
[2]Department of Earth and Planetary Sciences, Harvard University, Cambridge, Massachusetts, USA.

0094-8276/11/2011GL046769

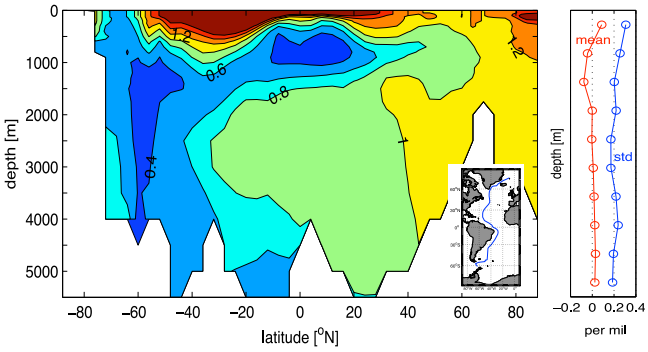

Figure 1. A check of the skill of the TMI method. (left) Section of estimated δ^{13}C from the TMI method along the western Atlantic GEOSECS track (inset map). (right) The mean difference (red) and standard deviation of the misfit (blue) between the TMI estimate and observations, calculated in 500 meter bins, and plotted as a function of depth.

method [*Lawson and Hanson*, 1974], we solve the matrix equation at each location: $\mathbf{Ex} + \mathbf{n} = \mathbf{y}$, where $\mathbf{E}$ is a square matrix, $\mathbf{n}$ is noise, and $\mathbf{y}$ is the observations. The weighting accounts for data accuracy, and the non-negativity constraint enforces mass contributions and nonconservative sources to be zero or greater. The local information is aggregated into a single matrix equation, $\mathbf{Ac} = \mathbf{d}$, where $\mathbf{A}$ contains the m's from the local inversion, $\mathbf{c}$ is any tracer distribution, and $\mathbf{d}$ provides the surface boundary conditions and interior source terms. The global matrix $\mathbf{A}$ is square, full rank, and encapsulates the influence of any ocean grid box on any other.

[6] The principles underlying TMI are straightforward, but several complexities must be dealt with. To account for the effects of the seasonal cycle, we apply TMI to observations that represent late wintertime conditions by requiring that the ocean be well-mixed above the seasonally-maximum mixed-layer depth, as this depth is most indicative of the properties transmitted into the ocean interior [*Stommel*, 1979]. Longer-term variations due to natural ocean-atmosphere variability and anthropogenic changes [*Johnson and Orsi*, 1997; *Curry and Mauritzen*, 2005] are treated by allowing uncertainty in the surface tracer concentrations that are explicitly solved for. In the rare (<0.01%) case that climatological tracer distributions do not provide enough independent information, we seek the circulation with the minimum amount of diapycnal mixing that still fits the observations. Furthermore, small-scale pathways along the ocean bottom are crucial for obtaining a realistic circulation, and thus, sub-gridscale bottom flows off of continental shelves and through mid-ocean fracture zones are allowed (see *Gebbie and Huybers* [2010] for more detail).

[7] We train TMI with the WOCE climatology of temperature, salinity, phosphate, nitrate, and oxygen [*Gouretski and Koltermann*, 2004] and the GISS oxygen-18/oxygen-16 isotope ratio [*LeGrande and Schmidt*, 2006] resolved at 2° × 2° in the horizontal and 33 levels in the vertical. The result is a steady-state circulation estimate that fits the 1,746,936 tracer observations within their reported uncertainties (see Figure S1 in auxiliary material).[1] As a more stringent test, we also analyze the consistency of this circulation estimate with a tracer distribution withheld from the inversion, the GEOSECS δ^{13}C observations [*Craig and Turekian*, 1980], where the influence of biological fractionation of carbon is accounted for by a 1.1‰ decrease in δ^{13}C for each 1 μmol/kg increase in phosphate [*Broecker and Maier-Reimer*, 1992]. The foregoing circulation estimate fits the withheld δ^{13}C observations to within a standard error of approximately 0.2‰ at each depth level, consistent with the expected measurement error and interlaboratory offsets inherent to the data (Figure 1), suggesting robustness. As a side benefit, TMI also yields a global estimate of the distribution of δ^{13}C that should be superior to standard estimates that assume isotropic spatial covariance. Additional tests of TMI using synthetic model data also indicate substantial skill (see the auxiliary material).

3. The Surface Origin of the Interior Ocean

[8] To estimate where all interior ocean waters were last in communication with the surface, we track backward along each pathway from the interior to the surface by means of an extension to the TMI methodology. The total volume, $\mathbf{V}_{tot}$, originating from a surface box could be calculated by dyeing the surface box and summing the product of the dye concentration and the volume of each gridbox. This calculation, however, is computationally intensive because each surface location must be dyed in succession, and instead we use the fact that $\mathbf{V}_{tot}$ is equal to the inverse transpose of the $\mathbf{A}$ matrix multiplied by a vector, $\mathbf{v}$, containing gridbox volumes: $\mathbf{V}_{tot} = \mathbf{A}^{-T}\,\mathbf{v}$. This expression is derived as a sensitivity or "adjoint" problem that gives all the relevant information in one calculation (see auxiliary material for the derivation).

[9] The number of surface origin sites that can be distinguished is only limited by the underlying spatial resolution of the dataset and independence of the observations at that resolution. One external parameter, the tapering coefficient α, is added to TMI to remedy any lack of independence in observations at 2° resolution. We find that the gridscale variability and degree of smoothness of Figure 2 is sensitive to this choice. Here, the strength of the tapering is deter-

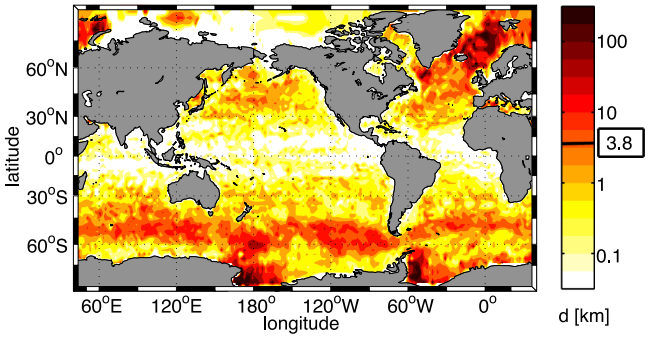

Figure 2. The surface sources of global ocean waters. Oceanic volume that has originated in each 2° by 2° surface location (11,113 origination sites), scaled by the surface area of each box to make an equivalent thickness, d. The color-scale follows a base-ten logarithm of the field. For reference, the colorbar includes the average depth of the ocean (3.8 km), equal to the area-weighted mean of d.

[1] Auxiliary materials are available in the HTML. doi:10.1029/2011GL046769.

Table 1. The Effective Endmembers That Fill the Ocean Averaged Into 7 Regions, and the Fraction of Ocean Property Variability Below 1000 Meters Depth That They Explain[a]

	ANT	NATL	SUBANT	NPAC	ARC	MED	TROP	11,113	7
θ [°C]	−1.31	2.64	5.09	5.43	−0.89	16.38	17.35	99.8	74.6
Sal. []	34.62	34.88	34.25	33.25	34.45	38.03	35.43	96.6	91.1
δ^{18}O [VSMOW]	−0.20	0.27	−0.21	−0.55	0.03	1.37	0.46	81.7	78.3
PO_4[$\mu mol/kg$]	2.11	0.84	1.62	1.41	1.09	0.13	0.45	99.1	98.8
NO_3[$\mu mol/kg$]	29.7	12.9	23.7	18.1	7.6	1.6	4.7	99.2	99.1
O_2[$\mu mol/kg$]	283	308	279	291	332	239	233	99.0	98.2

[a]The seven regions are the Antarctic, North Atlantic, Subantarctic, North Pacific, Arctic, Mediterranean, and Tropics (see auxiliary material for a map). The last two columns on the right-hand side indicate the percent variance explained for each property using the full TMI solution with 11,113 distinct origination sites, and that explained using seven effective endmembers. Note that PO_4, NO_3, and O_2 fractions are computed in both cases using the nonconservative effects estimated from TMI, whose importance accounts for the uniformly high fraction of variance explained.

mined by the signal-to-noise ratio in the tracer observations [*Hansen*, 1992], implemented so as to minimize diapycnal mixing while guarding against fitting noise in the observations (see the auxiliary material for details).

[10] Our estimate of the origin of interior waters averages across all production and destruction of waters over the equilibration time of the ocean—from decades to millennia depending upon location—and is, therefore, complementary to other estimates of water-mass formation that focus on seasonal and interannual timescales [e.g., *Khatiwala et al.*, 2002]. While water-mass formation rates have been previously estimated on a regional basis, such as the Southern Ocean [e.g., *Orsi et al.*, 1999, 2002], we produce a map on a global scale where the relative contributions are assessed in a consistent framework. Furthermore, we emphasize that TMI produces an estimate of effective formation, the net effect of formation and destruction, which is the relevant quantity for assessing global inventories on climatic timescales. As expected, important sites for filling the ocean exist in the North Atlantic, Weddell Sea, and Ross Sea (Figure 2). A prolific band of source regions also exists around the Antarctic Circumpolar Current, near 55°S, in accord with the documented importance of Subantarctic Mode Water and Antarctic Intermediate Water in ventilating the Southern Hemisphere [e.g., *McCartney*, 1977; *Piola and Georgi*, 1982]. Even though these Subantarctic waters have a relatively low density, they are irreversibly mixed with waters originating from the Antarctic region and upwelled waters originating from the North Atlantic. Once mixed, their journeys throughout the world ocean are intertwined and, thus, relatively light waters can have a significant presence at great depths [*Worthington*, 1981]. The estimated high contribution from regions of the Arctic, such as the Barents Sea, is sensitive to the assumed depth of the mixed layer. Note that contact with the atmosphere does not necessarily imply complete equilibration with overlying atmospheric conditions so that water properties may be indicative of exchanges at multiple locations, though for purposes of specificity we focus on the most recent exchange.

[11] While the interior ocean is made up of waters from many different surface sites, just a few property combinations may explain much of the ocean interior, as recognized by many previous water-mass studies [e.g., *McCartney and Talley*, 1982; *Johnson*, 2008]. A major issue is the choice of the properties themselves and interpreting what they mean. Here, TMI permits calculation of the most representative properties for a particular surface region, where the "effective endmembers" are given by the surface concentrations weighted by the volume filled by each location. Splitting the surface ocean into 7 regions (given by Figure S2 in the auxiliary material), we find that the North Atlantic surface region is characterized by $\theta = 2.64$°C and S = 34.88, while the Antarctic region is $\theta = -1.31$°C and S = 34.62, values that are similar to those traditionally used to describe NADW and AABW (see Table 1 for a complete list of endmembers). To determine how well the 7-region solution can explain interior tracer distributions, we propagate the endmember values into the interior by use of the regional water-mass fraction maps of *Gebbie and Huybers* [2010]. The TMI method with 11,113 surface sites explains 99.8% of the global temperature variability below 1000 meters depth, while the 7 endmember solution explains 74.6%, an adequate amount for many applications. For salinity, 96.6% of the variance is explained by the 11,113 surface sites, whereas 91.1% is explained by the 7 endmembers. Although a large number of surface sites fill the ocean, the number of property combinations that are needed to explain the majority of ocean tracer variability is much smaller.

4. Power-Law Description of Ocean Filling

[12] The percentage of water filled from a given surface site clearly depends on the spatial resolution of the dataset, so our results are discussed in terms that take surface area into account. We estimate that 85% of the ocean volume originates from 15% of the global surface area, a ratio reminiscent of the 80–20 rule-of-thumb (or Pareto principle) in statistics. When TMI is applied to the dataset that is block-averaged at 4° horizontal resolution, the estimate is very similar at 86%–14%. To display the spatial pattern of how the ocean is filled, we introduce an equivalent thickness, d, defined as the filled volume of the interior ocean divided by the area of a given surface patch. By definition, the average d across all surface points equals the average depth of the ocean. When ranked from largest to smallest, the equivalent thickness filled from successive surface patches follows a simple power-law distribution,

$$d_n = d_o n^{-p}, \tag{1}$$

where d_o equals 9.2×10^7 m, the d_n are arranged from largest to smallest, and n ranges from 1 to 11,113. Equation (1) is known as a Zipf distribution [*Newman*, 2005], and a maximum likelihood estimate [*Clauset et al.*, 2007] gives $p = 1.09 \pm 0.03$ (Figure 3, top). The estimate is statistically valid for the first 1,250 points, i.e., $n = 1250$ (black line in Figure 3, top). The distribution of d_n falls off more rapidly than n^{-p} for

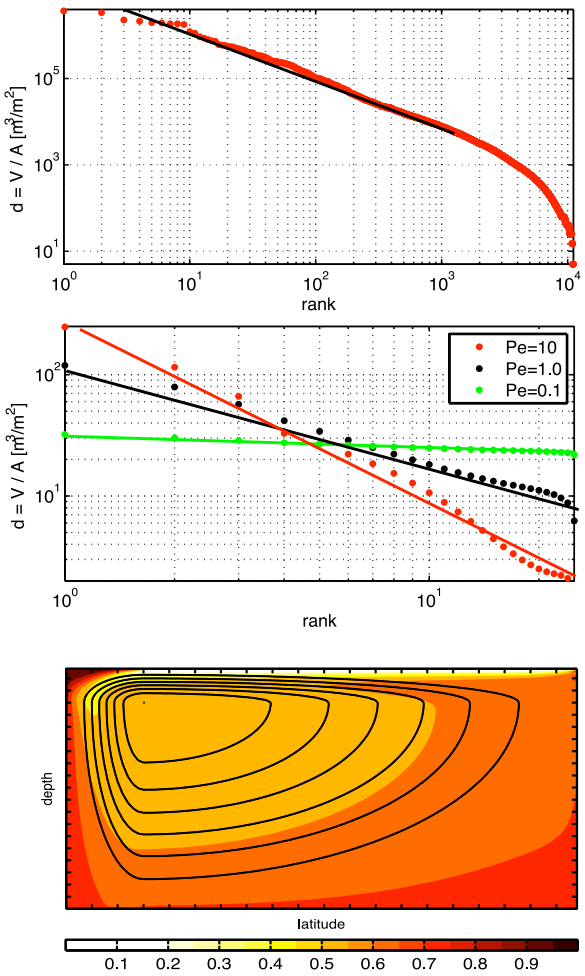

Figure 3. The distribution of volume contributions from 11,113 surface sites. (top) The distribution of equivalent thickness ordered from largest to smallest (red dots) with the best-fit power law (black line). If the x-axis is replaced by the cumulative fraction of ocean area, the plot is not visibly changed. (middle) A rank-size diagram of the same form as the top panel, but for an idealized advection-diffusion model of an overturning circulation. (bottom) The overturning streamfunction (black lines) of the idealized model with the fraction of water originating from the left-most five surface gridpoints (background color).

$n > 1250$. One could also fit the 100 most important points with a power law with a shallower slope closer to $p = 1$, although it does not have the statistical significance of our first fit. Repeating the analysis at 4° × 4° resolution results in a similar distribution once differences in surface area are accounted for (see Figure S3 in auxiliary material), reflecting the scale invariance associated with power-law processes.

[13] Some further insight into the controls upon the equivalent thickness distribution can be obtained from a simple tracer model containing an advective two-dimensional overturning cell and horizontal diffusion. The model produces a power-law scaling in equivalent thickness similar to that of the observations (Figures 3, middle and 3, bottom). The power-law slope is a function of the model's Peclet number; for example, decreasing the rate of advection relative to diffusion increases the breadth of surface sources entrained in downwelling fluid and gives a flatter distribution of d_n. Entrainment of diffusively mixed ambient fluid is expected from dynamical studies of ocean convection [*Jones and Marshall*, 1993] and gravity currents [*Hughes and Griffiths*, 2006]. Even if the advective velocity field indicates a small sinking region, it is possible to have a wide range of contributing surface regions.

5. Discussion and Conclusions

[14] The interpretation of the ocean as being filled by just a handful of sinking regions [*Stommel and Arons*, 1960; *Stommel*, 1962] was an idealized construct, and there is observational evidence for at least a few tens of waters that fill the ocean [e.g., *Gordon*, 1974; *Talley and Raymer*, 1982; *McCartney and Talley*, 1982; *Hanawa and Talley*, 2001; *Yashayaev and Clarke*, 2008]. Nonetheless, numerical tools for dealing with more than ten water masses have been lacking, essentially requiring observational studies to assume just a few surface regions contribute to filling the interior [e.g., *Stuiver et al.*, 1983; *Matsumoto*, 2007]. Here we quantify how the ocean is filled at 2° resolution through the inversion of most of the available ocean tracer data. Prior to this work, only numerical models [*Haine and Hall*, 2002; *Primeau*, 2005] or data assimilation products [e.g., *Schlitzer*, 2007] could provide a picture of how the ocean is filled at this resolution.

[15] Furthermore, we find that the volume filled by each surface box generally follows a power-law distribution, when ranked from highest to lowest. The shallow slope of the power law, which we suggest is set by the ratio of advective and diffusive processes, indicates that the ocean is filled from a broad number of surface locations. Specifically, 15% of the ocean surface fills 85% of the interior. Nonetheless, it is possible to describe much of the variability in interior property distributions using small numbers of property combinations due to regional homogeneities. The power-law scaling of ocean filling is rather simple given the various controls upon water formation, including brine rejection in polar regions, gravitational instability of deep water formation in subpolar regions, and wind-induced subduction in the subtropics. It will be useful to explore the degree to which this power law holds in the presence of changes in ocean energetics, stratification, and bathymetry. The more detailed quantification of the relationship between surface properties and the interior composition of the ocean should also facilitate study of how variations in interior water-mass properties [e.g., *Johnson et al.*, 2007] relate to surface climate.

[16] **Acknowledgments.** GG and PH were funded by NSF award 0645936. GG was also supported by the J. Lamar Worzel Assistant Scientist Fund and the Penzance Endowed Fund in Support of Assistant Scientists. PH was also supported by NSF award OCE-0960787. We thank Carl Wunsch, Andrew Rhines, Luke Skinner, and two anonymous reviewers for constructive comments. We also thank Bruce Warren for his feedback and dedicate this work to him.

[17] The Editor thanks two anonymous reviewers for their assistance in evaluating this paper.

References

Anderson, L. A., and J. L. Sarmiento (1994), Redfield ratios of remineralization determined by nutrient data analysis, *Global Biogeochem. Cycles*, *8*(1), 65–80.

Broecker, W. S., and E. Maier-Reimer (1992), The influence of air and sea exchange on the carbon isotope distribution in the sea, *Global Biogeochem. Cycles*, *6*(3), 315–320.

Broecker, W. S., et al. (1998), How much deep water is formed in the Southern Ocean?, *J. Geophys. Res.*, *103*(C8), 15,833–15,843.

Clauset, A., C. Shalizi, and M. Newman (2007), Power-law distributions in empirical data, *SIAM Rev.*, *51*(4), 661–703.

Craig, H., and K. K. Turekian (1980), The GEOSECS program—1976–1979, *Earth Planet. Sci. Lett.*, *49*(2), 263–265.

Curry, R., and C. Mauritzen (2005), Dilution of the northern North Atlantic Ocean in recent decades, *Science*, *308*(5729), 1772–1774.

Gebbie, G., and P. Huybers (2010), Total matrix intercomparison: A method for resolving the geometry of water-mass pathways, *J. Phys. Oceanogr.*, *40*(8), 1710–1728.

Gordon, A. (1974), Varieties and variability of Antarctic Bottom Water, *Colloq. Int. C. N. R. S.*, *215*, 33–47.

Gouretski, V., and K. Koltermann (2004), WOCE global hydrographic climatology, *Tech. Rep. 35*, Ber. des Bundesamtes für Seeschifffahrt und Hydrogr., Hamburg, Germany.

Haine, T. W. N., and T. M. Hall (2002), A generalized transport theory: Water-mass composition and age, *J. Phys. Oceanogr.*, *32*(6), 1932–1946.

Hanawa, K., and L. Talley (2001), Mode waters, in *Ocean Circulation and Climate: Observing and Modelling the Global Ocean*, *Int. Geophys. Ser.*, vol. 77, pp. 373–386, Academic, San Diego, Calif.

Hansen, P. C. (1992), Analysis of discrete ill-posed problems by means of the L-curve, *SIAM Rev.*, *34*(4), 561–580.

Hughes, G., and R. Griffiths (2006), A simple convective model of the global overturning circulation, including effects of entrainment into sinking regions, *Ocean Modell.*, *12*(1–2), 46–79.

Johnson, G. C. (2008), Quantifying Antarctic Bottom Water and North Atlantic Deep Water volumes, *J. Geophys. Res.*, *113*, C05027, doi:10.1029/2007JC004477.

Johnson, G. C., and A. H. Orsi (1997), Southwest Pacific Ocean water-mass changes between 1968/69 and 1990/91, *J. Clim.*, *10*(2), 306–316.

Jones, H., and J. Marshall (1993), Convection with rotation in a neutral ocean: A study of open-ocean deep convection, *J. Phys. Oceanogr.*, *23*, 1009–1039.

Khatiwala, S., P. Schlosser, and M. Visbeck (2002), Rates and mechanisms of water mass transformation in the Labrador Sea as inferred from tracer observations, *J. Phys. Oceanogr.*, *32*(2), 666–686.

Lawson, C. L., and R. J. Hanson (1974), *Solving Least-Squares Problems*, Prentice Hall, Englewood Cliffs, N. J.

LeGrande, A. N., and G. A. Schmidt (2006), Global gridded data set of the oxygen isotopic composition in seawater, *Geophys. Res. Lett.*, *33*, L12604, doi:10.1029/2006GL026011.

Mackas, D. L., K. L. Denman, and A. F. Bennett (1987), Least squares multiple tracer analysis of water mass composition, *J. Geophys. Res.*, *92*(C3), 2907–2918.

Matsumoto, K. (2007), Radiocarbon-based circulation age of the world oceans, *J. Geophys. Res.*, *112*, C09004, doi:10.1029/2007JC004095.

McCartney, M. (1977), Subantarctic mode water, in *A Voyage of Discovery: George Deacon 70th Anniversary Volume, Supplement to Deep-Sea Research*, edited by M. V. Angel, pp. 103–119, Pergamon, Oxford, U. K.

McCartney, M., and L. Talley (1982), The subpolar mode water of the North Atlantic Ocean, *J. Phys. Oceanogr.*, *12*(11), 1169–1188.

Newman, M. (2005), Power laws, Pareto distributions and Zipf's law, *Contemp. Phys.*, *46*(5), 323–351.

Orsi, A. H., G. C. Johnson, and J. L. Bullister (1999), Circulation, mixing, and production of Antarctic Bottom Water, *Prog. Oceanogr.*, *43*(1), 55–109.

Orsi, A. H., W. M. Smethie Jr., and J. L. Bullister (2002), On the total input of Antarctic waters to the deep ocean: A preliminary estimate from chlorofluorocarbon measurements, *J. Geophys. Res.*, *107*(C8), 3122, doi:10.1029/2001JC000976.

Piola, A., and D. Georgi (1982), Circumpolar properties of Antarctic Intermediate Water and Subantarctic Mode Water, *Deep Sea Res., Part A*, *29*(6), 687–711.

Primeau, F. (2005), Characterizing transport between the surface mixed layer and the ocean interior with a forward and adjoint global ocean transport model, *J. Phys. Oceanogr.*, *35*(4), 545–564.

Schlitzer, R. (2007), Assimilation of radiocarbon and chlorofluorocarbon data to constrain deep and bottom water transports in the world ocean, *J. Phys. Oceanogr.*, *37*(2), 259–276.

Stommel, H. (1962), On the smallness of sinking regions in the ocean, *Proc. Natl. Acad. Sci. U. S. A.*, *48*(5), 766–772.

Stommel, H. (1979), Determination of water mass properties of water pumped down from the Ekman layer to the geostrophic flow below, *Proc. Natl. Acad. Sci. U. S. A.*, *76*, 3051–3055.

Stommel, H., and A. B. Arons (1960), On the abyssal circulation of the world ocean. II. An idealized model of the circulation pattern and amplitude in oceanic basins, *Deep Sea Res.*, *6*, 217–233.

Stuiver, M., P. D. Quay, and H. G. Ostlund (1983), Abyssal water C-14 distribution and the age of the world oceans, *Science*, *219*(4586), 849–851.

Talley, L. D., and M. E. Raymer (1982), Eighteen degree water variability, *J. Mar. Res.*, *49*, 755–775.

Tomczak, M. (1981), A multi-parameter extension of temperature/salinity diagram techniques for the analysis of non-isopycnal mixing, *Prog. Oceanogr.*, *10*(3), 147–171.

Tomczak, M. (1999), Some historical, theoretical and applied aspects of quantitative water mass analysis, *J. Mar. Res.*, *57*(2), 275–303.

Tomczak, M., and D. G. B. Large (1989), Optimum multiparameter analysis of mixing in the thermocline of the eastern Indian Ocean, *J. Geophys. Res.*, *94*(C11), 16,141–16,149.

Warren, B. A. (1981), Deep circulation of the world ocean, in *Evolution of Physical Oceanography, Scientific Surveys in Honor of Henry Stommel*, edited by B. A. Warren and C. Wunsch, pp. 6–41, MIT Press, Cambridge, Mass.

Worthington, L. (1981), The Water Masses of the World Ocean: Some Results of a Fine-Scale Census, in *Evolution of Physical Oceanography, Scientific Surveys in Honor of Henry Stommel*, edited by B. A. Warren and C. Wunsch, pp. 42–60, MIT Press, Cambridge, Mass.

Wüst, G. (1935), Schichtung und zirkulation des Atlantischen Ozeans. Die stratosphare, in *The Stratosphere of the Atlantic Ocean*, edited by W. J. Emery, pp. 1–180, U.S. Dep. of Commer., Springfield, Va.

Yashayaev, I., and A. Clarke (2008), Evolution of North Atlantic water masses inferred from Labrador Sea salinity series, *Oceanography*, *21*(1), 30–45.

G. Gebbie, Woods Hole Oceanographic Institution, MS 29, Woods Hole, MA 02543, USA. (ggebbie@whoi.edu)

P. Huybers, Department of Earth and Planetary Sciences, Harvard University, Cambridge, MA 02138, USA.